Double blind ultrafast pulse characterization by mixed frequency generation in a gold antenna

Sylvain D. Gennaro[1], Yi Li[1], Stefan A. Maier[1,2] and Rupert F. Oulton[1†]

[1]*The Blackett Laboratory, Department of Physics, Imperial College London, London SW7 2AZ, UK*
[2]*Chair in Hybrid Nanosystems, Nanoinstitute Munich, Faculty of Physics, Ludwig-Maximilians-Universität München, München, Germany*

†Corresponding author: r.oulton@ic.ac.uk

Ultrafast pulse characterization requires the analysis of correlation functions generated by frequency mixing of optical pulses in a nonlinear medium. In this work, we use a gold optical nanoantenna to generate simultaneously Four Wave Mixing and Sum Frequency Generation across the tuning range of a Ti: Sapphire and Optical Parametric Oscillator (OPO) system. Since metal nanoparticles create remarkably strong nonlinear responses for their size without the need for phase matching, this allows us to simultaneously characterize the unknown OPO pulse and its pump pulse using a single spectrogram. The nonlinear mixing is efficient enough to retrieve pulses with energies in the picojoule range.

Keywords: Plasmonics. Nonlinear Optics. Ultrashort Pulse Characterization. Nano-antennas. Sum Frequency Generation. Four Wave Mixing.

Introduction

Ultrashort pulse characterization such as Frequency Resolved Optical Gating (FROG)[1,2] or Spectral Phase Interferometry (SPIDER)[3] requires gating a number of optical pulses in a nonlinear medium. A two dimensional time versus wavelength spectrogram is compiled based on either third order [2] or second order[4] correlation signals and analyzed by an algorithm that reconstructs pulse shapes in time. The characterization of multiple unknown ultrafast pulses has been possible using either a technique called Double Blind FROG[5,6], or by using multiple nonlinear processes of the same order, e.g. SHG and Sum Frequency Generation[7]. In these techniques, the number of nonlinear processes involved dictates how many ultrashort pulses can be simultaneously retrieved. However, phase matching in a single nonlinear crystal will limit the types of nonlinear processes achievable and the spectral range where they can be efficient.

Plasmonic optical antennas[8] offer a promising route toward ultrathin nonlinear devices with little limitation on phase matching[9,10]. These metallic nanostructures sustain strong resonant electromagnetic fields via electronic charge oscillations at their surfaces [11], which can simultaneously generate second (SHG)[12–16] and third harmonic generation(THG)[17–19], Sum Frequency Generation[20](SFG) and Four Wave Mixing (FWM)[21–23] with interaction lengths shorter than the optical wavelength.

In this work, we exploit degenerate Four Wave Mixing (FWM) and Sum Frequency Generation (SFG) signals from an individual gold antenna to characterize two near IR ultrafast optical pulses from a Coherent Chameleon Optical Parametric Oscillator (OPO) without the need of a known reference pulse. The multi-resonant antenna is designed to exhibit two dipolar resonances between 1300-1500 nm (Bar) and between 700–840 nm (Disks), which define the operating range of the retrieval technique[16]. The FWM, and SFG responses may span a bandwidth of 400+nm over the input tuning range allowing us to produce spectrograms of the various mixing processes simultaneously. We are able to retrieve the pulse chirp and spectra assuming secant square pulses shapes of our two near IR ultrafast optical pulses, demonstrating the viability of the technique.

Linear characterization

We begin by examining the linear optical responses of our optical antennas. Each antenna consists of a gold bar and two gold discs (See scanning electron micrograph (SEM) in the inset of Figure 1a), with resonances detuned by about an octave, in this case near 1500 nm and 750 nm for the bar and disks, respectively. The linear extinction spectra of Figure 1b and 1d, measured with Fourier transform infrared (FTIR) microscope (See methods section for more details) are for arrays of antenna and show the resonances of the disks and bar. The bar resonance requires an input polarization parallel to its long axis, but the disks show clear extinction for either polarization. However, for polarized excitation perpendicular to the bar (Figure 1d), the disks' extinction spectrum in the range of 700 nm - 850 nm exhibits a dip. This is attributed to a resonant near field coupling or "Fano" interference effect between the dipolar mode of the disks and a less-radiative second order mode of the bar. The coupling is controlled by the relatively narrow gaps (<20nm) between the disks and the bar within each antenna[16]. It is this coupling phenomenon that facilities the various nonlinear mixing processes.

Lumerical simulations of the electric field, displayed in Figures 1c and 1e, confirm the required polarizations to excite the bar and disk modes. However, when considering frequency mixing between wavelengths accessed by the two resonant elements of each antenna, a strong mutual field overlap is required. In this work, we show that nonlinear frequency mixing occurs principally in the bar element as it simultaneously sustains resonant modes at both the *pump* and *signal* frequency. For more information on the simulation, see the method section of this article.

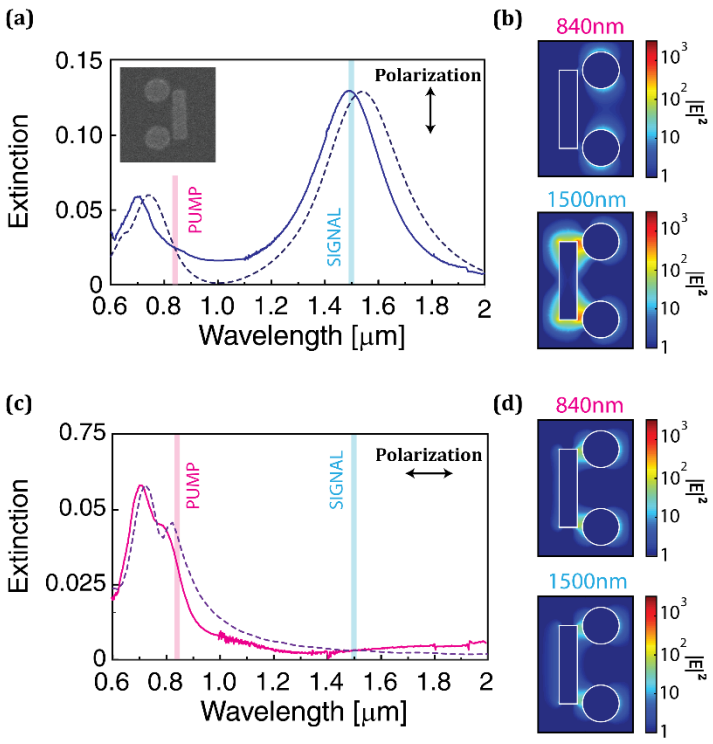

Fig. 1. Linear characterization of the multi-resonant gold nanoantenna. (a, c) The measured FTIR (solid lines) and simulated (broken color lines) extinction spectra for light incident parallel (x-axis) and perpendicular (y-axis) to the bar, respectively. Inset: SEM of the nanoantenna. Dimension of the bar is 340×80×40 nm3 in x, y and z respectively, while disks are the same thickness with diameters of 140 nm. The gaps between the disks and the bar are 20 nm. (b, d) The logarithmic scale of normalized electric field distribution is represented at the wavelength of the pump at 840 nm and the signal at 1500 nm. The bar and the disk coupled to each other via near field coupling. Nonlinear characterization

In our nonlinear experiments, the longitudinal dipolar resonance of the bar is accessible via a *signal* beam with a wavelength between 1200 nm - 1600 nm, while the dipolar resonance of the disks is accessed via *pump* beam with wavelengths in the range 700 nm - 850 nm. Any two *pump* (ω_2) and *signal* (ω_1) frequencies were selected to be close to the design resonance wavelengths within the limitations of our Chameleon Optical Parametric Oscillator pumped by a Chameleon Ultra II laser system. The experimental apparatus is described in the method section and Figure S1 of the supplementary information. Both beams were focussed onto an individual antenna as much as possible given the restrictions of chromatic aberration[24]. Figure 2a and 2b plot the nonlinear up-conversion processes of photons when our antenna is excited with two temporally-overlapping femtosecond laser pulses. A variety of nonlinear processes are evident including Third Harmonic Generation (THG) of the *signal* beam, Four Wave Mixing (FWM) ($2\omega_1 - \omega_2 = \omega_3$) and Sum Frequency Generation (SFG) ($\omega_1 + \omega_2 = \omega_4$), which are polarized predominantly along the bar. The nonlinear responses are the strongest for the configuration when the pump beam at frequency ω_2 excites the disk with a polarization orthogonal to the bar, and the signal beam at frequency ω_1 excites the bar with a polarization parallel to the bar. Here ω_1 optimally excited the bar, while ω_2 excites the Fano interference mode that links the responses of the bar and disks. For the inverse polarization configuration, the nonlinear response becomes much weaker, showing that the nonlinear processes is activated by the Fano interference effect. The obtained responses for the cases when both input beams are parallel to each other are presented in Supplementary Figures S2b and S2c, and lead to fairly equal but weak FWM with negligible SFG. The reader should note that the increasing broadband nonlinear response observed for longer wavelengths might come from two photon luminescence[25], to electronic inelastic light scattering[26], or more likely, to intraband absorption of gold [27,28]

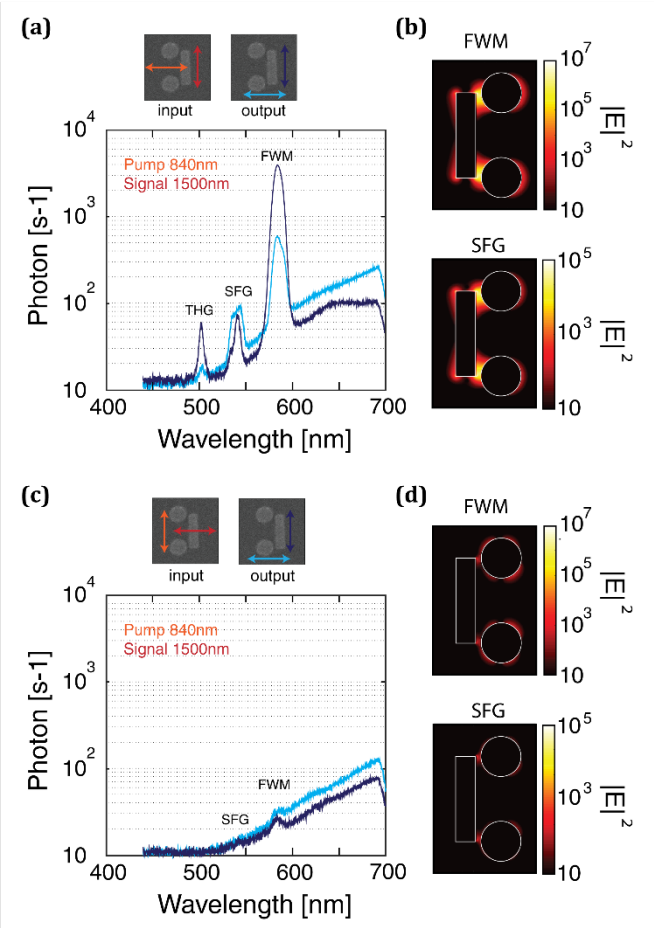

Fig. 2. Nonlinear characterization of an individual multi-resonant gold nanoantenna. (a, b) Logarithmic spectra of the nonlinear signal of an individual nanostructure for two input cross – polarized configurations at respectively 840 nm and 1500 nm. Cyan (resp. navy blue) is for an output polarization perpendicular (resp. parallel) to the bar. See Supplementary Figure S2 for the four different cases of input polarizations. (c, d) Calculated nonlinear (FWM and SFG) normalized electric field intensity distribution (in logarithmic scale) of a single antenna assuming an isotropic polarization. See method section and supplementary figure 3 and 4 for more information.

Numerical calculations support these observations. Figure 2c and 2d show the near-field electric intensity distributions for both FWM and SFG upon assuming an isotropic second and third order polarization. The nonlinear field enhancement is the strongest for the first polarization configuration as expected from their linear surface charge distribution shown in Figure 1b and d. For more information on the simulation, see the method section of this article and Supplementary Figure S3 and S4.

For non-zero time delay between the signal and pump larger than the pulse widths of our laser system (~100-200 fs), we only observe THG, confirming that the observed peaks are due to SFG and FWM processes. (See Supplementary Figure S5). Moreover, the FWM signal remains present while the signal wavelength is tuned from 1200 nm to 1600 nm, with a peak response of the FWM at 1400 nm. This can be attributed to the resonance of the bar which enables broadband far field coupling of the input beam to the plasmonic structure for a broad range of wavelengths (See Supplementary Figure S6a). In the visible, the interband absorption of gold limits SFG signal below 510nm (See Supplementary Figure S6b). This could be overcome by working with aluminum antennas [26]. The reader should also note that generally, the centrosymmetry of gold causes even order nonlinearity to be extremely weak; however, in metallic antennas, broken symmetry over the large surface area to volume ratio enables a significant second-order nonlinear response, which depends on the nonlinear surface charge polarization and the linear modal electric field[15,29]. Careful engineering of the radiation pattern can enhance the emission of the second order signal, which is typically only minimally radiative[16].

1. Nonlinear conversion efficiency

Figure 3 confirms the nature of nonlinear signal mixing, by plotting the collected up-converted responses as a function of powers of the pump (P_p) and signal (P_s) beams and identifying the power law, $\propto P_p^{n_p} P_s^{n_s}$. Sum Frequency Generation being a second order nonlinear process exhibits a linear dependence on the input power of both the *signal* and *pump* beams, where value of $n_s = 1.1$ and $n_p = 1$ are found. Meanwhile, Four Wave Mixing being a third order nonlinear process, exhibits a quadratic dependency on the *pump* power ($\lambda_1 = 840nm$) and a linear dependency on *signal* power ($\lambda_1 = 1500\ nm$), where $n_p = 1.8$ and $n_s = 0.9$ were found. We note that THG generates the expected cubic dependence on input power. For these data, we can quantify the efficiency of each nonlinear process. In particular, the nonlinear efficiency of SFG at 538nm is $\eta_{SFG} > 4.10^{-9}$, which gives a second-order susceptibility $\chi^{(2)}(\omega_4 = \omega_1 + \omega_2; \omega_1, \omega_2) > 70\ pm \cdot V^{-1}$ at 538nm. The nonlinear efficiency of FWM at 583nm is $\eta_{FWM} > 8.10^{-8}$, giving a third-order susceptibility $\chi^{(3)}(\omega_3 = 2\omega_1 - \omega_2; \omega_1, \omega_1, -\omega_2) > 30\ nm^2 \cdot V^{-2}$. (See Supplementary Notes S7 and S8 for the efficiency calculation).

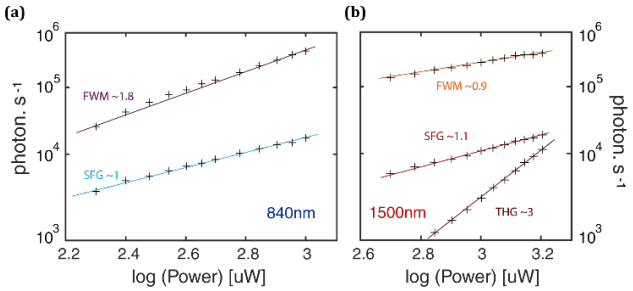

Fig. 3. Nonlinear photon per second versus input power in logarithmic scale for the various nonlinear processes. (a) The power of the *pump* beam at 840nm is varied. (b) The power of the *signal* beam at 1500 nm is varied. The various nonlinear processes have their respective expected polynomial power trends.

It is difficult to compare these values with those from the literature, since evaluating the second order susceptibility for gold is non-trivial. However, the third order susceptibility for Four Wave Mixing near 800nm for gold is $\chi^{(3)}(2\omega_1 - \omega_2; \omega_1, \omega_1, -\omega_2) \approx 0.2\ pm^2 \cdot V^{-2}$[30]. These data show that a resonantly-enhanced nonlinearity of a single antenna outperforms bulk gold by approximately a hundred fold.

Ultrashort pulse characterization

We now examine the temporal variation of the nonlinear signal. Figure 4a show a typical nonlinear spectrogram i.e. a 2D spectral intensity map of relative delay versus wavelengths, created by temporally- scanning the pump and signal laser pulses by 1um (6.6fs) step, and recording a spectra with 1s integration time at each scan delay. The map is then assembled by combining all the spectra to its respective delay positions. This essentially creates a FROG trace. In theory, the spectrogram in Figure 4a contains information on the pulse shape and duration of both incoming pulses and could therefore be retrieved without the use of any reference pulses. Here, we merely show that pulse retrieval is viable by assuming a hyperbolic secant squared pulse shape and retrieving the pulse chirp and spectrum. The pulse shape was inferred from fitting a variety of common pulse shapes (Gaussian, hyperbolic secant, Lorentzian), and selecting the one that gave the best match to the features in the measured spectrogram. Here, hyperbolic secant was chosen as the retrieved spectrogram reproduced the diamond-like trace as seen in our measured spectrogram (Fig 4.a.). Moreover, this is a pulse shape typically characteristic of ultrafast Ti: Sapphire laser systems.The retrieved second order spectral phase in the frequency domain accounts only for the group delay dispersion. From the two trial time-dependent electric fields, we create a spectrogram containing both FWM and SFG signal, and compare it to the measured spectrogram via a nonlinear least square nonlinear regression. See Supplementary Note S9 and S10 for a detailed description of the fitting algorithm

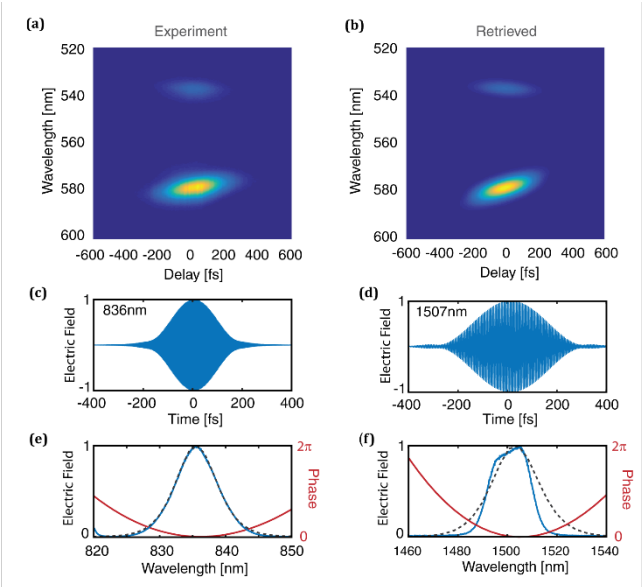

Fig. 4. Double Blind Ultrashort Pulse Characterization. (a) Experimental (b) Retrieved 2D spectrogram of wavelength versus delay displaying the FWM and SFG trace of an individual antenna. (c) 836nm (d) 1507nm time – dependent normalized electric field amplitude. (e) 836nm (f) 1507 normalized electric field amplitude spectrum. The blue solid line is the measured spectrum with our Acton 2300 spectrometer. The grey dash line is the retrieved spectrum from the model and the red solid line is the second order phase also referred as "chirp".

Figure 4b show the extracted spectrograms from the fitting procedure. While the overall orientation and shape matches the experiment, the experiment FWM and SFG trace is broader than the retrieved spectrogram. This might be due to the nonlinear effect of Self Phase Modulation or Four Wave Parametric mixing[31,32] not included in our model. Figure 4c and d shows the time – dependent retrieved electric field of two pulses of our laser system, with respective pulse durations of $\tau_{837nm} \leq 146$ fs and $\tau_{1505nm} \leq 228$ fs, which are in agreement with the manufacturer's specifications, and within the Time-Bandwidth limitation of our laser system (See Supplementary Figure S9). Figure 4e and f show the respective spectra of the retrieved pulses from our fitting procedure, plotted on top of the actual measured spectra of our laser pulses. Since both pulses have travelled to normally dispersive materials, the measured chirp is positive as expected. It is worth mentioning that our model only retains up to second order dispersion, since the higher order terms, produced an asymmetric distortion of the retrieved FWM and SFG spectrograms that did not match the experimental traces. We also aimed to include self-phase modulation in our model by adding a time-intensity dependent phase in the time domain. However, this produced a retrieved spectral response with broader tails than the spectra that were measured directly. The poorer correspondence of the retrieved near IR pulse spectrum to that observed, could be due to distortions of the measured spectrum by filters.

Inhomogeneity in nanoparticle size of an antenna's array could lead to local phase variations which might distort the wavefronts of the various nonlinear signals. However, these metal nanostructures have fairly broad resonances, as they are designed to have as large a radiative loss rate as possible, and so inhomogeneous broadening is small. We note that phase distortions due to the resonators would amount to a maximum pi phase change across the nanostructure bandwidth. Since the spectral width of the nonlinear responses is more than an order of magnitude less than spectral width of the nanostructures, the small variations in nanoparticle size will only have a minor effect on the nonlinear spectral width, and the phase of the pulse. The role of inhomogeneity would become significant when the pulse duration requires a bandwidth comparable to the nanostructures resonance – at this point, plasmonic dephasing would distort the pulse characterization. Since the plasmon dephasing time [33–37] is on the order of 10fs which limits this pulse characterization method to pulses durations longer than a few tens of femtoseconds. Here, we work in the few hundreds femtoseconds regime, where pulse durations of transform limited pulses is significantly greater than the plasmonic dephasing time, enabling us to characterize the laser pulses themselves.

Conclusion

In conclusion, second-order and third-order frequency mixing processes (Sum Frequency Generation and Four Wave Mixing) are generated in a gold nanoantenna and used to characterize two unknown ultrafast pulses simultaneously. We observe strong nonlinear responses of $\eta_{FWM} = 8 \times 10^{-8}$ and $\eta_{SFG} > 4 \times 10^{-9}$ due to the

antenna design and plasmonic local field enhancement. The efficiency means that pulse characterization is possible for ~100 fs pulses in the picojoule pulse energy range. The relaxation of phase-matching condition enables multiple order nonlinear processes to be present, which enables simultaneous characterization of multiple pulses without the need of additional beam lines. Furthermore, the technique can be implemented at the focus of high numerical aperture integrated microscopy systems, where the micrometer-scale Rayleigh range would otherwise limit the effectiveness of nonlinear crystals.

Methods**Nanofabrication.** The gold nanoantennas were fabricated by electron beam lithography on borosilicate cover glass substrates. Firstly, the substrate was coated with a positive resist (PMMA) and was baked at 180 °C for at least 180 seconds. Then the geometries of nanoantennas were defined by an electron beam exposure at 20 keV, followed by a conventional MIBK:IPA development procedure. Subsequently, a 1.5 nm thick Cr film was deposited by thermal evaporation on the substrate (to increase the Au adhesion) followed by 40 nm Au film. Lift-off process in acetone and oxygen plasma ashing were adapted before optical measurements.

Linear characterization. Linear spectroscopic of the fabricated nanoparticle arrays were carried out with a Bruker Hyperion 2000 Fourier transform infrared (FTIR) microscope installed with a 36X, NA = 0.5 objective. The extinction (1 - transmission) spectra were obtained by normalizing the transmittance curve from an array of optical antennas with a reference spectrum taken from the substrate. Spectra were obtained in the ranges 500-1100 nm and 1100–2000 nm using a Silicon detector and Peltier cooled InGaAs detector, respectively.
Simulation. Numerical studies of the electromagnetic responses were performed using the finite-difference time-domain (FDTD) commercial software (Lumerical FDTD Solutions 2017a) with normal incidence. The top-view geometries were adjusted to closely match SEM images, and the heights were exactly the Cr and Au thickness deposited during sample fabrication. Charge density was obtained by calculating the difference of the normal component of the electric field above and below the Au surface (Gauss's law).
Optical set-up. For the nonlinear measurement, the nanostructure is pumped by nominally >140 fs optical pulses at 840nm and 1500nm respectively, generated by the signal from a Coherent-APE Chameleon OPO, seeded by a Coherent Chameleon Ultra II. Multiple dielectric filters are used to remove any undesirable wavelengths; for the visible *pump* beam at 840nm, a 750nm (FELH750) cut off long pass filters and an 850nm (FESH850) cut off short pass filters from Thorlabs are used to suppress any lower and higher wavelengths that might emerge from the oscillator; for the near IR *signal* beam, a 1000nm (FELH1000) cut off long pass filter is used. The linear polarization of each beam is rotated with two achromatic half wave plates: an AHWP05M-980 and an AHWP05M-1600 respectively. A dichroic mirror with a cut off wavelength of 1000nm (DMSP1000) selectively combines the two beams onto the sample. After the sample, the *pump* and *signal* are rejected by a 1000 nm (FESH1000), a 750nm (FESH750) and a 700nm (FESH700) cut off short pass filters. The nonlinear signal is collimated toward the entrance slit of a spectrometer (Acton2300). For all our measurement, our microscope objectives are two Nikon S Plan Fluor ELWD 40X 0.6NA. The output polarization of the nonlinear signal is selected via a linear polarizer (LPVIS100-MP2).

Funding. EPSRC Reactive Plasmonic Programme grant (EP/M013812/1); EPSRC Prize Doctoral Fellowship RGP-2016064. Leverhule Research Project Grant RPG-2016-064.

Acknowledgment. S.A.M. further acknowledges the Lee-Lucas Chair in Physics.

The author declares no competing financial interests.

Supporting Information Available: additional description of optical set-up, nonlinear simulation and description of the fitting algorithm are described. This material is available free of charge via the Internet at http://pubs.acs.org

REFERENCES

(1) Kane, D. J.; Trebino, R. Single-Shot Measurement of the Intensity and Phase of an Arbitrary Ultrashort Pulse by Using Frequency-Resolved Optical Gating. *Opt. Lett.* **1993**, *18* (10), 823–825.

(2) Delong, K. W.; Fittinghoff, D. N.; Trebino, R.; Kohler, B.; Wilson, K. Pulse Retrieval in Frequency-Resolved Optical Gating Based on the Method of Generalized Projections. *Opt. Lett.* **1994**, *19* (24), 2152–2154.

(3) Iaconis, C.; Walmsley, I. A. Spectral Phase Interferometry for Direct Electric-Field Reconstruction of Ultrashort Optical Pulses. *Opt. Lett.* **1998**, *23* (10), 792.

(4) Delong, K. W.; Trebino, R.; Hunter, J.; White, W. E. Frequency-Resolved Optical Gating with the Use of Second-Harmonic Generation. *J. Opt. Soc. Am. B* **1994**, *11* (11), 2206.

(5) Wong, T. C.; Ratner, J.; Trebino, R. Simultaneous Measurement of Two Different-Color Ultrashort Pulses on a Single Shot. *J. Opt. Soc. Am. B* **2012**, *29* (8), 1889.

(6) Wong, T. C.; Ratner, J.; Chauhan, V.; Cohen, J.; Vaughan, P. M.; Xu, L.; Consoli, A.; Trebino, R. Simultaneously Measuring Two Ultrashort Laser Pulses on a Single-Shot Using Double-Blind Frequency-Resolved Optical Gating. *J. Opt. Soc. Am. B* **2012**, *29* (6), 1237.

(7) Kida, Y.; Nakano, Y.; Motoyoshi, K.; Imasaka, T. Frequency-Resolved Optical Gating with Two Nonlinear Optical Processes. *Opt. Lett.* **2014**, *39* (10), 3006.

(8) Novotny, L.; Van Hulst, N. F. Antennas for Light. *Nat. Photonics* **2011**, *5* (2), 83–90.

(9) Krasnok, A.; Tymchenko, M.; Alù, A. Nonlinear Metasurfaces: A Paradigm Shift in Nonlinear Optics. *Mater. Today* **2017**, 1–14.

(10) Li, G.; Zhang, S.; Zentgraf, T. Nonlinear Photonic Metasurfaces. *Nat. Rev. Mater.* **2017**, *2* (5), 17010.

(11) Maier, S. A. *Plasmonics: Fundamentals and Applications*; Springer-Verlag Berlin: New York, 2010.

(12) Czaplicki, R.; Mäkitalo, J.; Siikanen, R.; Husu, H.; Lehtolahti, J.; Kuittinen, M.; Kauranen, M.; Makitalo, J.; Siikanen, R.; Hannu, H.; et al. Second-Harmonic Generation from Metal Nanoparticles: Resonance Enhancement versus Particle Geometry. *Nano Lett.* **2015**, *15* (1), 530–534.

(13) Metzger, B.; Gui, L.; Fuchs, J.; Floess, D.; Hentschel, M.; Giessen, H. Strong Enhancement of Second Harmonic Emission by Plasmonic Resonances at the Second Harmonic Wavelength. *Nano Lett.* **2015**, *15* (6), 3917–3922.

(14) Aouani, H.; Navarro-cia, M.; Rahmani, M.; Sidiropoulos, T. P. H.; Hong, M.; Oulton, R. F.; Maier, S. A. Multiresonant Broadband Optical Antennas As Efficient Tunable Nanosources of Second Harmonic Light. *Nano Lett.* **2012**, *12* (9), 4997–5002.

(15) Butet, J.; Brevet, P.-F.; Martin, O. J. F. Optical Second Harmonic Generation in Plasmonic Nanostructures: From Fundamental Principles to Advanced Applications. *ACS Nano* **2015**, *9* (11), 10545–10562.

(16) Gennaro, S. D.; Rahmani, M.; Giannini, V.; Aouani, H.; Sidiropoulos, T. P. H.; Navarro-Cía, M.; Maier, S. a.; Oulton, R. F. The Interplay of Symmetry and Scattering Phase in Second Harmonic Generation from Gold Nanoantennas. *Nano Lett.* **2016**, *16* (8), 5278–5285.

(17) Metzger, B.; Schumacher, T.; Hentschel, M.; Lippitz, M.; Giessen, H. Third Harmonic Mechanism in Complex Plasmonic Fano Structures. *ACS Photonics* **2014**, *1* (6), 471–476.

(18) Aouani, H.; Rahmani, M.; Navarro-Cía, M.; Maier, S. A.; Aouani, H.; Rahmani, M.; Navarro-cı, M. Third-

Harmonic-Upconversion Enhancement from a Single Semiconductor Nanoparticle Coupled to a Plasmonic Antenna. *Nat. Nanotechnol.* **2014**, *9* (4), 290–294.

(19) Navarro-Cia, M.; Maier, S. a. Broad-Band near-Infrared Plasmonic Nanoantennas for Higher Harmonic Generation. *ACS Nano* **2012**, *6* (4), 3537–3544.

(20) Sartorello, G.; Olivier, N.; Zhang, J.; Yue, W.; Gosztola, D. J.; Wiederrecht, G. P.; Wurtz, G.; Zayats, A. V. Ultrafast Optical Modulation of Second- and Third-Harmonic Generation from Cut-Disk-Based Metasurfaces. *ACS Photonics* **2016**, *3* (8), 1517–1522.

(21) Danckwerts, M.; Novotny, L. Optical Frequency Mixing at Coupled Gold Nanoparticles. *Phys. Rev. Lett.* **2007**, *98* (26104), 1–4.

(22) Zhang, Y.; Wen, F.; Zhen, Y.-R.; Nordlander, P.; Halas, N. J. Coherent Fano Resonances in a Plasmonic Nanocluster Enhance Optical Four-Wave Mixing. *Proc. Natl. Acad. Sci.* **2013**, *110* (23), 9215–9219.

(23) Simkhovich, B.; Bartal, G. Plasmon-Enhanced Four-Wave Mixing for Superresolution Applications. *Phys. Rev. Lett.* **2014**, *112* (5), 1–5.

(24) Gennaro, S. D.; Roschuk, T. R.; Maier, S. A.; Oulton, R. F. Measuring Chromatic Aberrations in Imaging Systems Using Plasmonic Nanoparticles. *Opt. Lett.* **2016**, *41* (7), 1688.

(25) Schuck, P. J.; Fromm, D. P.; Sundaramurthy, A.; Kino, G. S.; Moerner, W. E. Improving the Mismatch between Light and Nanoscale Objects with Gold Bowtie Nanoantennas. *Phys. Rev. Lett.* **2005**, *94* (1), 14–17.

(26) Hugall, J. T.; Baumberg, J. J. Demonstrating Photoluminescence from Au Is Electronic Inelastic Light Scattering of a Plasmonic Metal: The Origin of SERS Backgrounds. *Nano Lett.* **2015**, *15* (4), 2600–2604.

(27) Haug, T.; Klemm, P.; Bange, S.; Lupton, J. M. Hot-Electron Intraband Luminescence from Single Hot Spots in Noble-Metal Nanoparticle Films. *Phys. Rev. Lett.* **2015**, *115* (6), 1–5.

(28) Roloff, L.; Klemm, P.; Gronwald, I.; Huber, R.; Lupton, J. M.; Bange, S. Light Emission from Gold Nanoparticles under Ultrafast Near-Infrared Excitation: Thermal Radiation, Inelastic Light Scattering, or Multiphoton Luminescence? *Nano Lett.* **2017**, *17* (12), 7914–7919.

(29) O'Brien, K.; Suchowski, H.; Rho, J.; Salandrino, A.; Kante, B.; Yin, X.; Zhang, X.; Brien, K. O.; Suchowski, H.; Rho, J.; et al. Predicting Nonlinear Properties of Metamaterials from the Linear Response. *Nat. Mater.* **2015**, *14* (4), 379–383.

(30) Boyd, R. W.; Shi, Z.; De Leon, I. The Third-Order Nonlinear Optical Susceptibility of Gold. *Opt. Commun.* **2014**, *326*, 74–79.

(31) Yang, G.; Shen, Y. R. Spectral Broadening of Ultrashort Pulses in a Nonlinear Medium. *Opt. Lett.* **1984**, *9* (11), 510–512.

(32) Agrawal, G. P.; Olsson, N. A. Self-Phase Modulation and Spectral Broadening of Optical Pulses in Semiconductor Laser Amplifiers. *IEEE J. Quantum Electron.* **1989**, *25* (11), 2297–2306.

(33) Lamprecht, B.; Krenn, J. R.; Leitner, A.; Aussenegg, E. R. Resonant and off-Resonant Light-Driven Plasmons in Metal Nanoparticles Studied by Femtosecond-Resolution Third-Harmonic Generation. *Phys. Rev. Lett.* **1999**, *83* (21), 4421–4424.

(34) Lamprecht, B.; Leitner, A.; Aussenegg, F. R. Invited Paper SHG Studies of Plasmon Dephasing in Nanoparticles. **1999**, *423*, 419–423.

(35) Kravtsov, V.; Ulbricht, R.; Atkin, J. M.; Raschke, M. B. Plasmonic Nanofocused Four-Wave Mixing for Femtosecond near-Field Imaging. *Nat. Nanotechnol.* **2016**, *11* (5), 459–464.

(36) Anderson, A.; Deryckx, K. S.; Xu, X. G.; Steinmeyer, G.; Raschke, M. B. Few-Femtosecond Plasmon Dephasing of a Single Metallic Nanostructure from Optical Response Function Reconstruction by

Interferometric Frequency Resolved Optical Gating. *Nano Lett.* **2010**, *10* (7), 2519–2524.

(37) Hanke, T.; Krauss, G.; Träutlein, D.; Wild, B.; Bratschitsch, R.; Leitenstorfer, A. Efficient Nonlinear Light Emission of Single Gold Optical Antennas Driven by Few-Cycle near-Infrared Pulses. *Phys. Rev. Lett.* **2009**, *103* (25), 1–4.

For Table of Contents Use Only

Double blind ultrafast pulse characterization by mixed frequency generation in a gold antenna

Sylvain D. Gennaro[1], Yi Li[1], Stefan A. Maier[1,2] and Rupert F. Oulton[1†]

[1]The Blackett Laboratory, Department of Physics, Imperial College London, London SW7 2AZ, UK
[2]Chair in Hybrid Nanosystems, Nanoinstitute Munich, Faculty of Physics, Ludwig-Maximilians-Universität München, München, Germany

†Corresponding author: r.oulton@ic.ac.uk

TOC Graphic

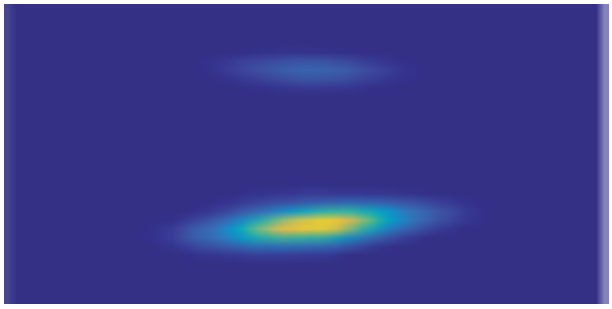

Frequency mixing of two optical pulses in a plasmonic antenna leads to a Four Wave Mixing, and Sum Frequency Generation spectrogram (wavelength versus delay), that contains information on the pulse shape and duration of both incoming pulses and could therefore be retrieved without the use of any reference pulses